Published in final edited form as:
Radiat Res. 2012 June ; 177(6): 804–812.

Microbeam Radiation Therapy Alters Vascular Architecture and Tumor Oxygenation and is Enhanced by a Galectin-1 Targeted Anti-Angiogenic Peptide

Robert J. Griffin[a,1], **Nathan A. Koonce**[a], **Ruud P. M. Dings**[b], **Eric Siegel**[d], **Eduardo G. Moros**[a], **Elke Bräuer-Krisch**[c], and **Peter M. Corry**[a]

[a]Department of Radiation Oncology, University of Arkansas for Medical Sciences, Little Rock, Arkansas

[b]Department of Biochemistry, Molecular Biology, Biophysics, University of Minnesota, Minneapolis, Minnesota

[c]European Synchrotron Radiation Facility, Grenoble, France

[d]Department of Biostatistics, University of Arkansas for Medical Sciences, Little Rock, Arkansas

Abstract

In this study, we sought to determine the therapeutic potential of variably sized (50 μm or 500 μm wide, 14 mm tall) parallel microbeam radiation therapy (MRT) alone and in combination with a novel anti-angiogenic peptide, anginex, in mouse mammary carcinomas (4T1) – a moderately hypoxic and radioresistant tumor with propensity to metastasize. The fraction of total tumor volume that was directly irradiated was approximately 25% in each case, but the distance between segments irradiated by the planar microbeams (width of valley dose region) varied by an order of magnitude from 150-1500 μm corresponding to 200 μm and 2000 μm center-to-center inter-microbeam distances, respectively. We found that MRT administered in 50 μm beams at 150 Gy was most effective in delaying tumor growth. Furthermore, tumor growth delay induced by 50 μm beams at 150 Gy was virtually indistinguishable from the 500 μm beams at 150 Gy. Fifty-micrometer beams at the lower peak dose of 75 Gy induced growth delay intermediate between 150 Gy and untreated tumors, while 500 μm beams at 75 Gy were unable to alter tumor growth compared to untreated tumors. However, the addition of anginex treatment increased the relative tumor growth delay after 500 μm beams at 75 Gy most substantially out of the conditions tested. Anginex treatment of animals whose tumors received the 50 μm beams at 150 Gy also led to an improvement in growth delay from that induced by the comparable MRT alone. Immunohistochemical staining for CD31 (endothelial cells) and aSMA (smooth muscle pericyte-associated blood vessels as a measure of vessel normalization) indicated that vessel density was significantly decreased in all irradiated groups and pericyte staining was significantly increased in the irradiated groups on day 14 after irradiation. The addition of anginex treatment further decreased the mean vascular density in all combination treatment groups and further increased the amount of pericyte staining in these tumors. Finally, evidence of tumor hypoxia was found to decrease in tumors analyzed at 1–14 days after MRT in the groups receiving 150 Gy peak dose, but not 75 Gy peak dose. Our results suggest that tumor vascular damage induced by MRT at these potentially clinically acceptable peak entrance doses may provoke vascular normalization and may be exploited to improve tumor control using agents targeting angiogenesis.

[1]Address for correspondence: Department of Radiation Oncology, University of Arkansas for Medical Sciences, Little Rock, Arkansas 72205; RJGriffin@uams.edu. .

INTRODUCTION

Previous studies have reported the effect of microbeam radiation therapy (MRT) in several tumor types and in a variety of settings (1–4). In the current study, we investigated the effects of single-array parallel-planar microbeams on treatment response. Two proportional patterns of beams were used: 50 μm wide with 200 μm center-to-center (ctc) distance or 500 μm wide with 2000 ctc distance. In addition, we studied the effect of combining antiangiogenic therapy with MRT on tumor vasculature, oxygenation and tumor growth. To our knowledge this is the first study of its kind.

MRT dedicated research efforts on pre-clinical models of cancer began about 20 years ago at Brookhaven National Laboratory (5). Since that time, several *in vivo* studies, most notably on 9LGS gliosarcoma, have been carried out at the European Synchrotron Radiation Facility (ESRF, Grenoble, France) (6–10). MRT involves administering very high entrance and peak doses (generally >100 Gy) of spatially fractionated synchrotron X rays. The technique was first developed as a prospective way to deposit high doses of ionizing radiation in inaccessible pediatric brain tumors while sparing normal CNS tissue. Some studies have suggested that the normal tissue-sparing phenomenon could be linked to radiation resistance of larger, more developmentally mature normal vessels containing smooth muscle and fully functional basement membrane to entrance doses up to 1000 Gy while a preferential effect on tumor microvasculature was observed (6, 11, 12). In contrast, Serduc *et al.* found a lack of tumor vessel damage in response to MRT up to 28 days. However, between these studies there are variances in the MRT parameters, and the earlier study suggest that MRT parameters need to be optimized to induce selective tumor vessel damage (10). In addition to microbeam size and spacing, valley dose and treatment geometry (unidirectional compared to bidirectional irradiation) and differences in beam spectrum, flux and collimation schemes used at different synchrotron facilities are all variables to be considered in analyzing the literature to date (13). In our study, we used irradiation parameters that have been previously established and a commonly studied murine breast cancer model (4T1) to assess the effect of adjuvant anti-angiogenic therapy. Cis-Pt, Temozolomide and Gd-DTPA are a few therapeutic agents that have been studied in combination with MRT to date (14). In recent years, the addition of anti-angiogenic compounds in radiation treatment has become an increasingly studied approach to improving tumor control as well as possibly impacting metastasis. We have demonstrated a significant therapeutic benefit of using vascular targeting/vascular disrupting agents on tumor radiation response (15, 16). One aspect of the mechanism by which radiation response is improved by these agents may be due to alterations in tumor oxygenation, and thus the tumor physiology and metabolic profile. We have observed antiangiogenic agents such as anti-VEGF antibody Avastin or a tumor endothelial cell binding peptide, anginex, can transiently normalize the vasculature and increase overall oxygenation in the tumor (17). The anginex peptide binds to galectin-1, an upregulated beta-galactoside-binding protein found in tumor-associated endothelial cells. During tumor angiogenesis, galectin-1 plays a role in activated endothelial cell migration and adherence to the extracellular matrix (18).

We hypothesized that in addition to antiangiogenic actions and modification of tumor physiology, the ability of vessel-targeting agents to inhibit vessel repair or reconnection following radiation damage may be a substantial factor in the anti-tumor effects observed with combination treatment of established tumors (19, 20). It has become increasingly clear that a major mechanism of action for high-dose irradiation is vascular damage (21–25). Therefore, since MRT has the inherent ability to cause precise and significant radiation damage along planar tracks, including vascular breakdown, the combination of MRT with angiogenesis inhibition might be highly-effective in controlling tumor progression.

MATERIALS AND METHODS

Cell Lines and Tumor Model

Mouse mammary tumor cells (4T1) were cultured at 378C and 5% CO_2 in DMEM/F12 50-50 (Mediatech Inc., Manassas, VA) supplemented with 10% BCS. Cells growing exponentially were harvested at 80% confluency with 0.15% trypsin and counted. Cells were spun down, washed in PBS, resuspended in serum free media at 2E5/0.05 ml and 50 μl aliquots were injected subcutaneously in the right rear limb of female Balb/c mice. Animals were shipped to the European Synchrotron Radiation Facility (ESRF, Grenoble, France) 6 days after implantation. Protocols for animal use were approved by both the French Authority on animal use for research at ESRF and the University of Arkansas for Medical Sciences (Little Rock, AR) Animal Care and Use Committee (IACUC).

Microbeam Radiation Therapy and Dosimetry

Tumors reached approximately 7 × 10 mm in diameter by day 10 and were randomized into 9 treatment groups: control (untreated), 50 μm beam width/200 μm ctc, 150 Gy or 75 Gy with and without anginex and 500 μm beam width/2000 μm ctc 150 Gy or 75 Gy with and without anginex. MRT was performed using beamline ID17 at the European Synchrotron Radiation Facility (ESRF), Grenoble, FR (http://www.esrf.eu/). Ultra-relativistic electrons circulating in a storage ring emit X rays on a tangent to the ring. The wiggler magnet produces a spectrum of photons from 50 to 350 keV with a median energy of 90 keV that pass through a multi-slit collimator. The collimator separates the broad beam into quasi-parallel planar microbeams of defined width ranging from 25 μm to 1 mm in size. These spatially fractionated beams can deliver high doses resulting in desired dose deposition in the targeted tissue within fractions of a second, while nontargeted tissue benefits from the small beam divergence allowing step dose gradients. The irradiation setup for MRT necessitates a vertical scanning through the beam using a goniometer with the help of a computer controlled stage and a fast shutter system. This is because a high photon flux at an acceptable homogeneity can only be extracted in the central cone of the ID17 wiggler beamline, resulting in 40 mm beam width and 0.5 mm beam height at a distance of 43 m from the source (wiggler). As shown in Fig. 1A, the height of the beams was approximately 14 mm after collimation and the arrays contained on average eight 500 um beams or 75 beams of 50 um in width (Fig. 1C).

Anesthesia

Mice were anesthetized with 1.5–2.5% isofluorane for all MRT treatments and delivered with 100% oxygen at 1 L/min. Breathing was monitored via remote camera and anesthesia adjustments were made accordingly.

Anginex Administration

Anginex is a designed peptide based on several features of known endogenous inhibitors of angiogenesis with low toxicity, water solubility and long shelf life (26, 27). Anginex was administered at 20 mg/kg/day i.p. for 14 days with the first dose given 2 h before MRT exposure. The injections were alternated between the left and right side of the abdomen daily.

Immunohistochemistry

At the desired times, 60 mg/kg pimonidazole was i.p. injected (HPI, Burlington, MA). After 90 min, the animals were euthanized and tumors were removed and bisected perpendicular to the microbeam plane of radiation. Half was placed in OCT and frozen, half was fixed in 10% neutral buffered formalin and embedded in paraffin. Five micrometer sections were

immunostained with Hypoxyprobe-1 kit according to manufacturer recommendations and as described (17, 28). In brief, peroxidase quench with 3% H_2O_2 was followed by antigen retrieval at 908C for 20 min in Antigen Unmasking Fluid (ABD Serotec, Raleigh, NC), blocking with Dako Blocking Solution (Dako, Carpinteria, CA) for 10 min, application of primary antibody 1:50 (HPI, Burlington, MA) for 60 min followed by secondary antibody 1:100 (HPI, Burlington, MA) for 20 min, Diaminobenzidine (DAB) (Vector Laboratories, Burlingame, CA) for 10 min and counterstained with Gill's hematoxylin for 30 s. In a negative control sample, antibody diluent (Millipore, Billerica, MA) was used in place of primary antibody. Tissue staining was quantified with an Aperio Scanscope (Aperio, Vista, CA) at 20× magnification and analyzed using Imagescope software (Aperio, Vista, CA). Necrotic areas, tissue folds and borders were excluded from the analyses and remaining viable tissue was analyzed for DAB signal using an algorithm preconfigured to quantify brown coloration by intensity ranges (weak, medium, and strong). For detection of endothelial cells and smooth muscle actin, frozen sections were stained using PE-conjugated 1:50 anti-CD31 (BD Pharmingen, Sparks, MD) or fitc-conjugated 1:250 anti-alpha smooth muscle actin (aSMA), and counterstained with vectashield mounting medium with DAPI (Vector, Burlingame, CA). Multiple fields were imaged using a fluorescent microscope and the staining patterns were quantified using a custom-made software program as described by us and others (29, 30).

Morphometric Analysis

Preparation and procedures for the formalin fixed paraffin embedded tumors sections were performed as described earlier (17). Briefly, similar size tumors without apparent widespread necrosis were excised and fixed in 10% formaline, and subsequently embedded in parafilm. The tissues were cut in 5 μm sections, and after rehydration and antigen retrieval, the slides were stained for vessel density (CD31, BD PharMingen) in a 1:50 dilution or for pericytes (anti-alpha smooth muscle actin) in a 1:250 dilution, developed with DAB and lightly counterstained with hematoxylin (17). Images of the sections were acquired on Aperio Scanscope (Aperio, Vista, CA) at 20× magnification, and digitally analyzed and differentially quantified by morphometric analysis, as described earlier (17, 31, 32). Aside from vessel density (including number, size and length of vessels), this digital approach discriminates among vessel branch points, end points, and vessel length, and allows for quantification of these architectural parameters.(17, 31, 32) After binarization of the images, vessel and pericytes density was quantified by scoring the total number of white pixels per field, as previously described (17, 31, 32).

Statistical Analysis

Tumor volumes were calculated using the formula $a^2b/2$, where a and b are respectively the long and short tumor diameters measured using calipers. The volumes thereby obtained first were normalized by expressing them as ratios relative to their day 0 values, then transformed to their base-10 logarithms to facilitate inference on ratio changes, and analyzed via repeated-measures analysis using the Mixed Procedure in SAS v9.2 (the SAS Institute, Cary, NC). Because the equal-variance assumption was strongly violated even after $\log_{10}$ transformation, the repeated-measures autocovariance was (1) modeled as having heterogeneous first-order autoregressive structure within treatment groups, and (2) allowed to vary between treatment groups; denominator degrees of freedom was accordingly calculated via the Satterthwaite method. Repeated-measures *post hoc* analysis consisted exclusively of pairwise comparisons of treatments at each time point. For the immunohistochemistry data summarized in Table 2, pixel counts were compared for differences via two-sample Student's *t* test using Microsoft Excel 2007 (Microsoft Corporation, Redmond, WA). In both analyses, comparisons were two-sided and used a

significance level that was set at alpha = 0.05 despite the multiple comparisons, so as not to inflate Type II Error in this modestly powered study.

RESULTS

Dosimetry and Irradiation Setup

Table 1 illustrates the calculated and measured radiation doses. The average peak doses were 150 Gy at 5 mm depth while the measured valley doses in a 10 mm solid water phantom were found to be 7.5 Gy in the case of the 50 μm 200 ctc radiation pattern and 6.4 Gy for the 500 μm 2000 ctc configuration. All dose values can be scaled identically for the 75 Gy peak entrance dose. Figure 1A is an image of the two beam geometries captured on Gafchromic film as they exited the tumor volume. A magnification of the microbeam-exposed films is shown in Fig. 1B.

The dose in the homogenous field was measured with a thimble ionization chamber PTW semiflex 31002, positioned in the center of a 15 × 15 mm sized field at 5 mm depth in a solid water phantom. Correction factors for pressure, temperature and ion recombination were applied and resulted in a dose-rate value of 85 Gy/s/mA (the dose rate depends on the electron current in the Synchroton ring-gantry at any one moment). Depending on the geometries used, an output factor of 0.8 was applied in the macro for the 50 μm full width at half-maximum beam sizes, while an output factor of 0.92 was used in case of the 0.5 mm sized beams, ensuring peak entrance dose values of 150 Gy for both irradiation geometries. Monte Carlo calculations were made for the peak and valley doses assuming that the beams were perfectly parallel and the medium was water. Since these assumptions neglected geometrical and scattering effects from the source to the water medium, the valley dose was measured for the field sizes and parameters used at 10 mm depth within a solid water phantom by exposing Gafchromic films (HD-810) (ISP Technologies Inc., www. ispcorp.com), which were read out with the help of a microdensitometer (J.L. Automation) (33). Table 1 also includes the measured valley dose at 10 mm depth in a solid water phantom using an Epson scanner (V750 Pro) and a Joyce Loebl micro-densitometer (34, 35). The Monte Carlo calculated relative profiles are shown in Fig. 1C.

Influence of Beam Size and Spacing on MRT-Induced Tumor Growth Delay

The growth rate after MRT therapy of 4T1 murine breast tumors with peak doses of either 75 Gy or 150 Gy parallel beam sizes of 50 μm (200 μm ctc), or 500 μm beams (2000 μm ctc) is shown in Fig. 2A and C. The average tumor volume was calculated for each treatment group on each day, and either the time required to grow to 4-fold or 2-fold of the average volume of each group on the day of irradiation was estimated from the curves. When irradiated with 500 μm beams at the lower peak dose of 75 Gy, 4T1 tumors did not differ in growth compared to untreated tumors, whereas 50 μm beams at a peak dose of 75 Gy delayed the time required for tumors to increase in average volume 4-fold by 5 days (1.71 times longer than control tumors). In the case of the 150 Gy peak dose, both 500 μm and 50 μm beams delayed the time required for a 2-fold increase in average tumor volume by 4 days (2.33 times longer than control tumors).

Enhancement of MRT-Induced Tumor Growth Delay with Anti-Angiogenic Peptide (Anginex) Treatment

As shown in Fig. 2B, MRT in 500 μm beams alone at 75 Gy had no effect on tumor growth, whereas the combination of anginex treatment starting 2 h prior to MRT and continuing daily injections thereafter delayed tumor growth to a rate similar to that obtained by 50 μm, 75 Gy beams alone. However, the addition of anginex to 50 μm MRT at 75 Gy had no additional effect on tumor growth delay (Fig. 2B). As illustrated in Fig. 2D, when the dose

was increased to 150 Gy, a contrasting result was observed. Anginex had no additional effect on tumor growth in the 500 μm, 150 Gy treatment in comparison to radiation alone, while anginex treatment further delayed tumor growth in the 50 μm, 150 Gy treatment group by at least 2-fold longer than the time required for tumors receiving radiation alone to grow to twice the starting size. The volume in combination-treated tumors had not reached twice that of the starting volume by the end of the experiment.

Effect of MRT Alone and/or Combined with Anginex on Tumor Blood Vessel Density and Composition

Tumors treated with the various MRT regimens with and without anginex treatment were harvested at 14 days after irradiation for histological analysis. Tumor sections were immunostained to determine possible changes in overall vessel density and/or changes in the composition of the vessels induced by the single- and combined-modality treatments. Figure 3 is a representative image of the changes in vessel density observed after MRT with and without anginex treatment. At both 75 Gy and 150 Gy alone, the vessel density was noticeably altered at 14 days after treatment and was further decreased in the mice that received anginex treatment, compared to untreated control tumors. In addition, the amount of pericyte staining was increased at day 14 in all irradiated groups compared to control. Furthermore, the addition of anginex treatment increased the pericyte presence significantly compared to MRT alone in all cases. Table 2 is a quantification and statistical analysis of the results for both vessel density and pericyte presence for all treatments studied. We have previously used this digital quantification method for numerous studies as described (15, 17).

Changes in Evidence of Tumor Hypoxia After 150 Gy MRT

One or two animals from each group were euthanized at several time points from each MRT beam size group. We observed little change from the mean control tumor pimonidazole staining intensity (41 ± 8 intensity units) in tumors treated with 75 Gy MRT (data not shown). However, as shown in Fig. 4, tumors treated with 150 Gy MRT demonstrated evidence of a substantial reduction of overall pimonidazole staining intensity from 1–14 days after MRT.

DISCUSSION

In the current study, microbeam radiation therapy (MRT) administered in 50 μm parallel planar beams with 200 μm ctc distance delayed tumor growth to a greater degree than MRT in 500 μm beams and 2000 μm ctc distance. The addition of daily treatment with the anti-angiogenic peptide anginex further delayed tumor growth for both the 50 μm and 500 μm beam sizes, but only in the high-dose (150 Gy) and low-dose (75 Gy) groups, respectively. Evidence of MRT-induced vascular density reduction and vascular normalization, as well as re-oxygenation was found in tumors exposed to MRT alone, particularly in the tumors treated with 150 Gy peak doses and 50 μm beams. The addition of anti-angiogenic treatment further increased evidence of vascular normalization in irradiated tumors, which suggests that these treatments may be useful to induce improved response to additional drug or radiation therapy.

As expected, the lowest peak dose (75 Gy) along with the widest spacing of the beams (2000 μm ctc) resulted in the lowest radiation-induced tumor response, while the highest peak dose (150 Gy) along with the closest spacing (200 μm ctc) resulted in the greatest degree of tumor control. This would agree with what may be expected from what we already know about tumor biology, especially in a fast-growing tumor such as the 4T1, and in recent studies comparing MRT beam sizes and tumor suppression (36). With 1.5 mm between

beams, the realized effect of the MRT exposure is likely covered up by tumor growth over and around the beam tracks, and this rapid recovery is likely enhanced at the 75 Gy peak dose where some cells or vasculature could have survived in the irradiated fields. We purposely irradiated an identical volume of tumor between our two beam geometries to control at least one variable (amount of tumor directly exposed to a given dose) in order to more easily compare differences in vascular effects of beam widths and spacing that were an order of magnitude apart.

When the anginex peptide was added to the treatment regimen, the greatest relative gain in treatment response was found in the regimen that utilized a 75 Gy peak dose and 1500 μm spacing between the fields. This result suggests that the peak dose may have been suboptimal to completely eradicate the endothelial cells inside of the irradiation fields, as discussed above. However, the blocking of angiogenic activity or weakening of endothelial cell viability by anginex treatment was able to inhibit the regrowth/ reconnection of the vasculature across and within the irradiated fields. This resulted in a net effect of boosting the overall tumor control to a level comparable to that obtained with a 75 Gy peak dose and closer spacing (150 μm between fields). In the case where peak dose was increased to 150 Gy, there was a clear improvement with anginex in tumor inhibition at the 50 μm beam level only. And, in the more widely spaced beams, there was not a noticeable improvement in tumor growth inhibition by anginex. This apparently contradictory result may be due to the fact that at the higher doses, irradiated fields are nearly sterilized by the radiation and therefore the anginex effect was only observed when the beams were more closely spaced, causing more widespread vessel damage. Indeed, recent studies have highlighted the major role that vessel damage plays in the response of various tissues to MRT, as well as the dependence of effect on the size of the microbeams (12, 36). In the case of the wider-spaced and higher-dose beams, anginex may only have a noticeable effect on the growth of tissue in the dose valleys since the direct field was likely mostly killed by the radiation alone. However, we know from previous work that anginex has rather small anti-tumor effects when used alone (15, 37, 38). Therefore, the negligible effects of anginex in combination with wider spaced and higher dose beams agree in principal with these previous results.

Another factor in our results could be the role of a bystander response to MRT. By nature, the microbeam geometry creates a very large surface area for these effects to be propagated, since the many beams traveling through tissue have two sides of surface area each equal to the height multiplied by the length of the tumor. There is abundant evidence now in the literature that radiation-induced bystander effects can be broadly classified into two types: those mediated by gap-junctions, requiring cell-to-cell communication and those brought about by the presence of factors secreted into the medium, which do not require cell-to-cell contact (39–44). In the case of the wide and narrow MRT beams studied here, there would be a large difference in the amount of surface area by which the cell-to-cell communication effect could be transmitted (50 μm beams with 200 μm ctc having a 10-fold greater surface area in tumors of identical shape and size). The secreted factor type of bystander effect would be less easily estimated, since we do not know how many cell layers the secreted factors can pass through or by which route the factors migrate. Nonetheless, recent work in our group using spatially fractionated conventional radiation, as well as in other laboratories looking at high-dose radiation therapy (45), has observed substantial bystander cell killing (50% increase or more) when single doses of 10 Gy or higher are applied. In the case of MRT, the doses in-beam are 10-fold higher than these. Therefore, it is reasonable to assume that there may be a bystander effect that contributes to the overall anti-tumor effect observed here and in the many other studies that have reported marked anti-tumor, as well as normal tissue, effects of MRT.

In addition to being the ultimate radiation sensitizer, improved tumor oxygenation has also been linked to immune function and chemotherapy response. Therefore, decreases in vessel density and induction of vascular normalization (pericyte presence), along with the apparent improvement in tumor oxygenation status observed post-treatment, suggests that MRT exposure could be useful to prime a patient's tumor for improved responses to chemotherapy, immunotherapy and/or radiation therapy. At least one other study indicated that MRT anti-tumor effects were stimulated by an immunotherapy approach (4).

MRT requires the availability of synchrotron facilities, which currently do not exist in enough locations to allow widespread clinical study. Alternatively, at our institution we have been steadily increasing the use of spatially fractionated radiotherapy applied with a linear accelerator for advanced head-and-neck cancer (48). Although the energies and scales of the beams are distinctly different between a light source and those produced by standard clinical equipment, significant gains in treatment response have been observed for both modalities, with little current knowledge on the mechanisms of action (1, 2, 4, 46, 47). Ongoing work in our group is centered on the use our new observations and understanding of MRT effects on tumor biology and response to therapy to qualitatively assist us in optimizing the use of spatially fractionated radiation as an adjuvant to currently employed treatment regimens. Therefore, further studies of a variety of spatially fractionated approaches alone, and in combination with agents that inhibit re-population and/or re-vascularization of the tumor, appear warranted.

Acknowledgments

This work was supported by the Central Arkansas Radiation Therapy Institute (CARTI), the European Synchrotron Radiation Facility, and NIH grant CA107160 to RJG. We thank Azemat Jamshidi-Parsian and Jessica Webber for assistance with tissue culture and animal handling prior to shipment to ESRF.

REFERENCES

1. Dilmanian FA, Button TM, Le Duc G, Zhong N, Pena LA, Smith JA, et al. Response of rat intracranial 9L gliosarcoma to microbeam radiation therapy. Neuro-Oncology. 2002; 4(1):26–38. [PubMed: 11772430]
2. Dilmanian FA, Morris GM, Zhong N, Bacarian T, Hainfeld JF, Kalef-Ezra J, et al. Murine EMT-6 carcinoma: high therapeutic efficacy of microbeam radiation therapy. Radiat Res. 2003; 159(5): 632–41. [PubMed: 12710874]
3. Dilmanian FA, Qu Y, Liu S, Cool CD, Gilbert J, Hainfeld JF, et al. X-ray microbeams: Tumor therapy and central nervous system research. Nuc Instrum Methods Phys Res. 2005; 548(1–2):30–7.
4. Smilowitz HM, Blattmann H, Brauer-Krisch E, Bravin A, Di Michiel M, Gebbers JO, et al. Synergy of gene-mediated immunoprophylaxis and microbeam radiation therapy for advanced intracerebral rat 9L gliosarcomas. J Neuro-Oncology. 2006; 78(2):135–43.
5. Slatkin DN, Spanne P, Dilmanian FA, Sandborg M. Microbeam radiation therapy. Med Phys. 1992; 19(6):1395–400. [PubMed: 1461201]
6. Bouchet A, Lemasson B, Le Duc G, Maisin C, Brauer-Krisch E, Siegbahn EA, et al. Preferential effect of synchrotron microbeam radiation therapy on intracerebral 9L gliosarcoma vascular networks. Int J Radiat Oncolo Biolo Phys. 2010; 78(5):1503–12.
7. Serduc R, Bouchet A, Brauer-Krisch E, Laissue JA, Spiga J, Sarun S, et al. Synchrotron microbeam radiation therapy for rat brain tumor palliation-influence of the microbeam width at constant valley dose. Phys Med Biol. 2009; 54(21):6711–24. [PubMed: 19841517]
8. Serduc R, Brauer-Krisch E, Bouchet A, Renaud L, Brochard T, Bravin A, et al. First trial of spatial and temporal fractionations of the delivered dose using synchrotron microbeam radiation therapy. J Synchro Radiat. 2009; 16(Pt 4):587–90.

9. Serduc R, Brauer-Krisch E, Siegbahn EA, Bouchet A, Pouyatos B, Carron R, et al. High-precision radiosurgical dose delivery by interlaced microbeam arrays of high-flux low-energy synchrotron X-rays. PLoS One. 2010; 5(2):e9028. [PubMed: 20140254]
10. Serduc R, Christen T, Laissue J, Farion R, Bouchet A, Sanden B, et al. Brain tumor vessel response to synchrotron microbeam radiation therapy: a short-term in vivo study. Phys Med Biol. 2008; 53(13):3609–22. [PubMed: 18560052]
11. Serduc R, Verant P, Vial JC, Farion R, Rocas L, Remy C, et al. In vivo two-photon microscopy study of short-term effects of microbeam irradiation on normal mouse brain microvasculature. Int J Radiat Oncolo Biolo Phys. 2006; 64(5):1519–27.
12. Sabatasso S, Laissue JA, Hlushchuk R, Graber W, Bravin A, Brauer-Krisch E, et al. Microbeam radiation-induced tissue damage depends on the stage of vascular maturation. Int J Radiat Oncol Biol Phys. 2011; 80(5):1522–32. [PubMed: 21740994]
13. Brauer-Krisch E, Serduc R, Siegbahn EA, Le Duc G, Prezado Y, Bravin A, et al. Effects of pulsed, spatially fractionated, microscopic synchrotron X-ray beams on normal and tumoral brain tissue. Mutat Res. 2010; 704(1–3):160–6. [PubMed: 20034592]
14. Regnard P, Brauer-Krisch E, Tropres I, Keyrilainen J, Bravin A, Le Duc G. Enhancement of survival of 9L gliosarcoma bearing rats following intracerebral delivery of drugs in combination with microbeam radiation therapy. Eur J Radiol. 2008; 68(3 Suppl):S151–5. [PubMed: 18635331]
15. Dings RP, Williams BW, Song CW, Griffioen AW, Mayo KH, Griffin RJ. Anginex synergizes with radiation therapy to inhibit tumor growth by radiosensitizing endothelial cells. Int J cancer. 2005; 115(2):312–9. [PubMed: 15688384]
16. Penagaricano J, Griffin R, Corry P, Moros E, Yan Y, Ratanatharathorn V. Spatially fractionated (GRID) therapy for large and bulky tumors. J Ark Med Soc. 2009; 105:263–5. [PubMed: 19475814]
17. Dings RP, Loren M, Heun H, McNiel E, Griffioen AW, Mayo KH, et al. Scheduling of radiation with angiogenesis inhibitors Anginex and Avastin improves therapeutic outcome via vessel normalization. Clin Cancer Res. 2007; 13(11):3395–402. [PubMed: 17545548]
18. Thijssen VL, Postel R, Brandwijk RJ, Dings RP, Nesmelova I, Satijn S, et al. Galectin-1 is essential in tumor angiogenesis and is a target for antiangiogenesis therapy. Proc Natl Acad Sci USA. 2006; 103(43):15975–80. [PubMed: 17043243]
19. Lee CG, Heijn M, di Tomaso E, Griffon-Etienne G, Ancukiewicz M, Koike C, et al. Anti-vascular endothelial growth factor treatment augments tumor radiation response under normoxic or hypoxic conditions. Cancer Res. 2000; 60(19):5565–70. [PubMed: 11034104]
20. Mauceri HJ, Hanna NN, Beckett MA, Gorski DH, Staba MJ, Stellato KA, et al. Combined effects of angiostatin and ionizing radiation in antitumour therapy. Nature. 1998; 394(6690):287–91. [PubMed: 9685160]
21. Garcia-Barros M, Paris F, Cordon-Cardo C, Lyden D, Rafii S, Haimovitz-Friedman A, et al. Tumor response to radiotherapy regulated by endothelial cell apoptosis. Science. 2003; 300(5622): 1155–9. [PubMed: 12750523]
22. Gorski DH, Beckett MA, Jaskowiak NT, Calvin DP, Mauceri HJ, Salloum RM, et al. Blockage of the vascular endothelial growth factor stress response increases the antitumor effects of ionizing radiation. Cancer Res. 1999; 59(14):3374–8. [PubMed: 10416597]
23. Gorski DH, Mauceri HJ, Salloum RM, Gately S, Hellman S, Beckett MA, et al. Potentiation of the antitumor effect of ionizing radiation by brief concomitant exposures to angiostatin. Cancer Res. 1998; 58(24):5686–9. [PubMed: 9865723]
24. Maj JG, Paris F, Haimovitz-Friedman A, Venkatraman E, Kolesnick R, Fuks Z. Microvascular function regulates intestinal crypt response to radiation. Cancer Res. 2003; 63(15):4338–41. [PubMed: 12907601]
25. Park H-J, Griffin RJ, Hui S, Song CW. Radiation-induced vascular damage in tumors: implications of vascular damage in ablative hypo-fractionated radiotherapy (SBRT and SRS). Radiat Res. (in press).
26. Mayo KH, van der Schaft DW, Griffioen AW. Designed beta-sheet peptides that inhibit proliferation and induce apoptosis in endothelial cells. Angiogenesis. 2001; 4(1):45–51. [PubMed: 11824378]

27. Dings RP, Mayo KH. A journey in structure-based drug discovery: from designed peptides to protein surface topomimetics as antibiotic and antiangiogenic agents. Acc Chem Res. 2007; 40(10):1057–65. [PubMed: 17661438]
28. Jankovic B, Aquino-Parsons C, Raleigh JA, Stanbridge EJ, Durand RE, Banath JP, et al. Comparison between pimonidazole binding, oxygen electrode measurements, and expression of endogenous hypoxia markers in cancer of the uterine cervix. Cytometry Part B, Clin Cytometry. 2006; 70(2):45–55.
29. Dings RP, Loren ML, Zhang Y, Mikkelson S, Mayo KH, Corry P, et al. Tumour thermotolerance, a physiological phenomenon involving vessel normalisation. Int J Hypertherm. 2011; 27(1):42–52.
30. Wild R, Ramakrishnan S, Sedgewick J, Griffioen AW. Quantitative assessment of angiogenesis and tumor vessel architecture by computer-assisted digital image analysis: effects of VEGF-toxin conjugate on tumor microvessel density. Microvasc Res. 2000; 59(3):368–76. [PubMed: 10792968]
31. Dings RP, Chen X, Hellebrekers DM, van Eijk LI, Zhang Y, Hoye TR, et al. Design of nonpeptidic topomimetics of antiangiogenic proteins with antitumor activities. J Natl Cancer Inst. 2006; 98(13):932–6. [PubMed: 16818857]
32. Dings RP, Van Laar ES, Webber J, Zhang Y, Griffin RJ, Waters SJ, et al. Ovarian tumor growth regression using a combination of vascular targeting agents anginex or topomimetic 0118 and the chemotherapeutic irofulven. Cancer Letters. 2008; 265(2):270–80. [PubMed: 18378392]
33. Nettelbeck H, Takacs GJ, Lerch ML, Rosenfeld AB. Microbeam radiation therapy: a Monte Carlo study of the influence of the source, multislit collimator, and beam divergence on microbeams. Med Phys. 2009; 36(2):447–56. [PubMed: 19291983]
34. Bräuer_Krisch E, Siegbahn EA, Bravin A. GafChromict film measurements for Microbeam Radiation Therapy (MRT). IFMBE Proceedings. 2009; 25 IFMBE:174–7.
35. Bräuer-Krisch, E.; Rosenfeld, A.; Lerch, M.; Petasecca, M.; Akselrod, GM.; Sykora, GJ., et al. MASR Proceedings. Melbourne, Australia: 2010. Potential High Resolution Dosimeters For MRT.
36. Uyama A, Kondoh T, Nariyama N, Umetani K, Fukumoto M, Shinohara K, et al. A narrow microbeam is more effective for tumor growth suppression than a wide microbeam: an in vivo study using implanted human glioma cells. J Synchro Radiat. 18(Pt 4):671–8.
37. Dings RP, Yokoyama Y, Ramakrishnan S, Griffioen AW, Mayo KH. The designed angiostatic peptide anginex synergistically improves chemotherapy and antiangiogenesis therapy with angiostatin. Cancer Res. 2003; 63(2):382–5. [PubMed: 12543791]
38. van der Schaft DW, Dings RP, de Lussanet QG, van Eijk LI, Nap AW, Beets-Tan RG, et al. The designer anti-angiogenic peptide anginex targets tumor endothelial cells and inhibits tumor growth in animal models. Faseb J. 2002; 16(14):1991–3. [PubMed: 12397082]
39. Mothersill C, Seymour CB. Radiation-induced bystander effects– implications for cancer. Nat Rev Cancer. 2004; 4(2):158–64. [PubMed: 14964312]
40. Hu B, Wu L, Han W, Zhang L, Chen S, Xu A, et al. The time and spatial effects of bystander response in mammalian cells induced by low dose radiation. Carcinogenesis. 2006; 27(2):245–51. [PubMed: 16150894]
41. Azzam EI, de Toledo SM, Little JB. Oxidative metabolism, gap junctions and the ionizing radiation-induced bystander effect. Oncogene. 2003; 22(45):7050–7. [PubMed: 14557810]
42. Azzam EI, de Toledo SM, Little JB. Direct evidence for the participation of gap junction-mediated intercellular communication in the transmission of damage signals from alpha-particle irradiated to nonirradiated cells. Proc Natl Acad Sci USA. 2001; 98(2):473–8. [PubMed: 11149936]
43. Azzam EI, Little JB. The radiation-induced bystander effect: evidence and significance. Hum Exp Toxicol. 2004; 23(2):61–5. [PubMed: 15070061]
44. Mothersill C, Seymour C. Radiation-induced bystander effects: past history and future directions. Radiat Res. 2001; 155(6):759–67. [PubMed: 11352757]
45. Butterworth KT, McGarry CK, Trainor C, O'Sullivan JM, Hounsell AR, Prise KM. Out-of-field cell survival following exposure to intensity-modulated radiation fields. Int J Radiat Oncol Biol Phys. 79(5):1516–22. [PubMed: 21277116]
46. Penagaricano JA, Moros EG, Ratanatharathorn V, Yan Y, Corry P. Evaluation of spatially fractionated radiotherapy (GRID) and definitive chemoradiotherapy with curative intent for locally

advanced squamous cell carcinoma of the head and neck: initial response rates and toxicity. Int J Rad Oncolo Biolo Phys. 76(5):1369–75.

47. Laissue JA, Geiser G, Spanne PO, Dilmanian FA, Gebbers JO, Geiser M, et al. Neuropathology of ablation of rat gliosarcomas and contiguous brain tissues using a microplanar beam of synchrotron-wiggler-generated X rays. Int J Cancer. 1998; 78(5):654–60. [PubMed: 9808538]
48. Asur RS, Sharma S, Whang C-W, Penagaricano P, Kommuru M, Moros EG. Spatially Fractionated Radiation Induces Cytotoxicity and Changes in Gene Expressionin Bystander and Radiation Adjacent Murine Carcinoma Cells. Radiat Res. 2012; 177:751–65. [PubMed: 22559204]

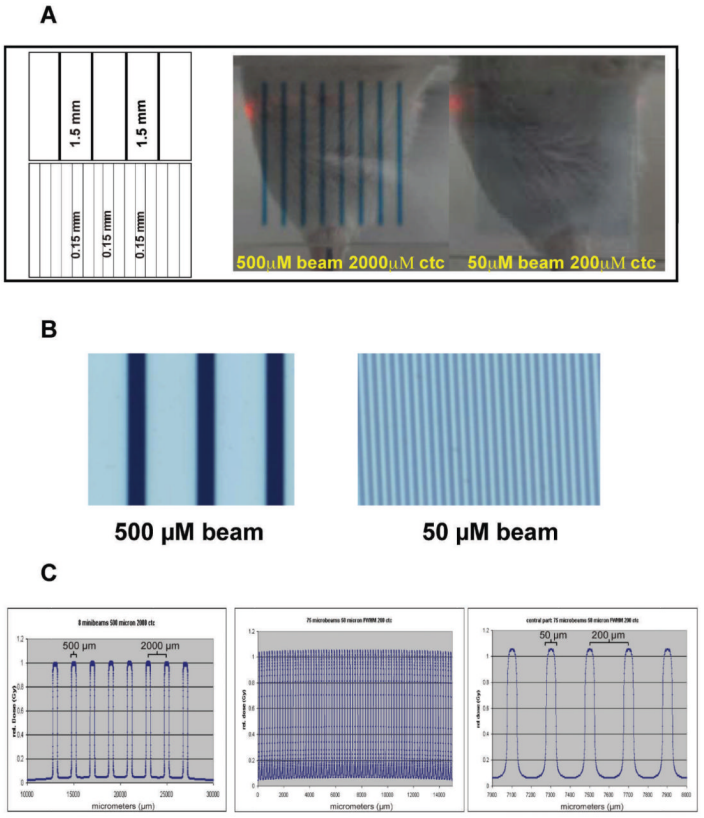

FIG. 1.

Panel A: A multi-slit collimator fractionates high-energy synchrotron X rays into parallel planar microbeams of variable beam sizes and spacing. In this experiment, 500 μm and 50 μm beams with 2000 μm and 200 μm center-to-center spacing, respectively, were generated (schematic, left side, not to scale). Gafchromic film captured the exit dose pattern for dosimetry and alignment (right side). Panel B: Magnification of the exit dose patterns for 500 μm and 50 μm beams with 1.5 mm and 0.15 mm spacing, respectively. Panel C: Relative dose plots from the Monte Carlo estimation for the MRT irradiation set-up. Left panel, 8 beams from the 500 μm beam pattern, middle panel, full spectrum of the 50 μm pattern, and, right panel, a section of the center portion of the 50 μm beam pattern.

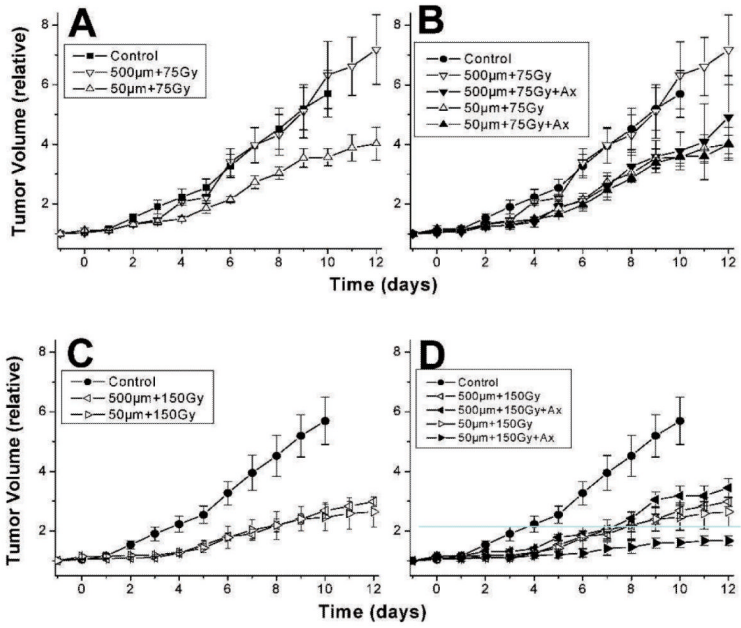

FIG. 2.

4T1 tumor growth after 75 Gy (panels A and B) or 150 Gy (panels C and D) alone or when combined with 20 mg/kg/day Anginex treatment starting 2 h before 500 μm or 50 μm MRT exposure and continuing until the end of observation. Each group contained 3–4 mice and the bars indicate 1 SEM. Tumors receiving MRT were all significantly delayed in tumor growth ($P < 0.01$) except for the 500 μm beam, 75 Gy group ($P=0.5$). When anginex treatment was added to MRT, there was a substantial change in tumor growth delay in the 500 μm, 75 Gy group (panel B), ($P=0.07$) and the 50 μm, 150 Gy group (panel D) ($P=0.06$). Tumor growth after 500 μm, 150 Gy or 50 μm, 75 Gy MRT was not altered with the addition of anginex treatment.

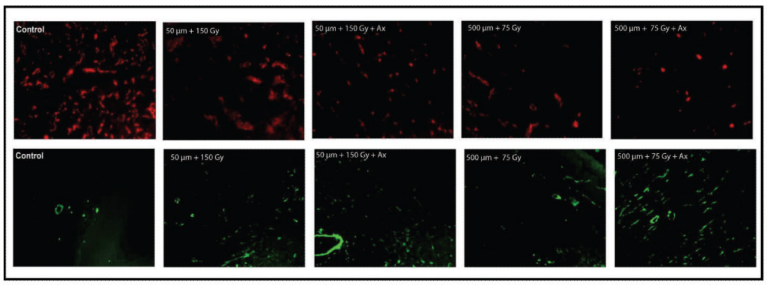

FIG. 3.

Examples of immunohistochemical staining of 4T1 tumor tissue for vessel density (anti-CD31, red) or pericytes (anti-αSMA, green). Mice were sacrificed at day 14 after MRT exposure and tumors were excised for staining and analysis.

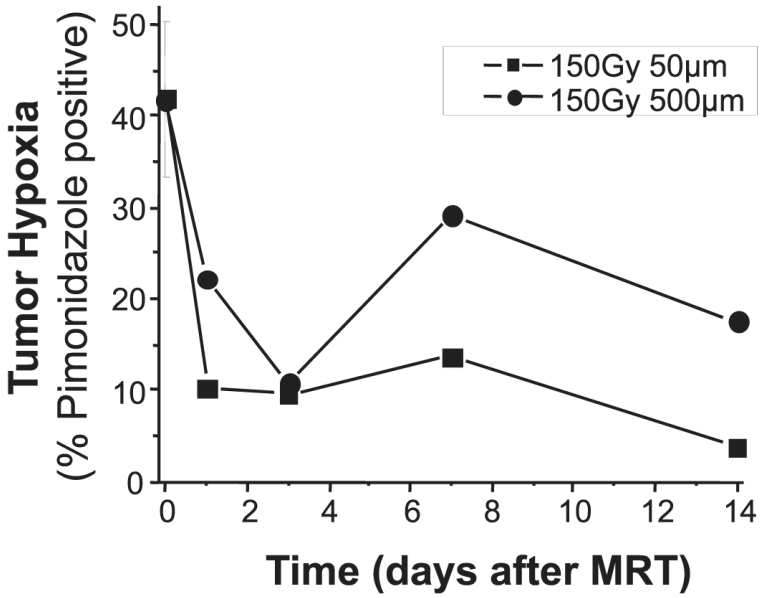

FIG. 4.

Pimonidazole positive staining in tumors over 2 weeks after MRT at 150 Gy peak dose with varying beam width. The average staining intensity from three untreated tumors is indicated at time 0, and the other time points are the average staining intensity of 1–2 tumors treated with each beam size.

TABLE 1

Beam Dosimetry

	50 μm, 200 ctc	**500 μm 2000 ctc**
Peak entrance dose (depth 0.5 mm)	150 ± 5 Gy	150 ± 5 Gy
Valley dose (Epson scanner) at 1 cm	8.8 ± 1 Gy	6.7 Gy ± 1 Gy
Valley dose (microdensitometer) at 1	7.5 ± 1 Gy	6.4 ± 1 Gy
Calculated valley dose (MC)	8.6 ± 0.5 Gy	7.4 Gy ± 0.5 Gy

TABLE 2

Histological Analysis of Microvessel and Pericyte Density

	Vessel density[a]	End points[b]	Branch points[c]	Vessel length[d]	Pericytes[c]
Control	12639 ± 697	435 ± 21.1	52 ± 4.8	58 ± 2.8	519 ± 180
50 μm + 150 Gy	8234 ± 736[f]	354 ± 27.1[g]	44 ± 5.0	41 ± 3.7[f]	1837 ± 514[g]
50 μm + 150 Gy + Ax	5732 ± 325[f,h]	237 ± 11.4[f,h]	18 ± 1.8[f,h]	24 ± 1.5[f,h]	4614 ± 428[g,i]
500 μm + 75 Gy	5456 ± 289[f]	229 ± 12.0[f]	32 ± 3.2[f]	26 ± 1.2[f]	2001 ± 336[g]
500 μm + 75 Gy + A	4760 ± 243[f,i]	210 ± 14.6[f]	23 ± 2.6[f,h]	23 ± 1.6[f]	3988 ± 933[g,i]

Note. Following binarization of images (magnification 200×; *n* 29–32 per group).

[a]Microvessel density was determined by scoring the total number of white pixels per field. Results show the mean white pixel count per image ± standard error.

[b]Mean number of vessel end points ± standard error as determined after skeletonization of the images.

[c]Mean number of vessel branch points/nodes per image in pixels ± standard error as determined after skeletonization of the images.

[d]Mean total vessel length per image in pixels ± standard error as determined after skeletonization of the images.

[e]Pericytes density was determined by scoring the total number of white pixels per field. Results show the mean white pixel count per image ± standard error.

[f]$P \leq 0.001$ or

[g]$P \leq 0.01$ (*t* test) Experimental group compared to vehicle.

[h]$P \leq 0.01$ or

[i]$P \leq 0.05$ (*t* test) Experimental groups compared ± anginex.